01 Jan 1985

Satellite Structure In Laser-assisted Charge-transfer Cross Sections

Y. P. Hsu

Ronald E. Olson
Missouri University of Science and Technology, olson@mst.edu

Recommended Citation

Y. P. Hsu and R. E. Olson, "Satellite Structure In Laser-assisted Charge-transfer Cross Sections," *Physical Review A*, vol. 32, no. 5, pp. 2707 - 2711, American Physical Society, Jan 1985.
The definitive version is available at https://doi.org/10.1103/PhysRevA.32.2707

Satellite structure in laser-assisted charge-transfer cross sections

Y. P. Hsu and R. E. Olson
Department of Physics, University of Missouri—Rolla, Rolla, Missouri 65401
(Received 28 May 1985)

A six-state coupled-channel calculation has been performed on the laser-assisted charge-transfer collision $H^+ + Na + \hbar\omega$. A greatly enhanced charge-transfer cross section is observed for low-energy collisions if the photon energy is matched to the classical satellite frequency. This frequency is determined by the location of an extremum in the difference of potential energies between the laser-pumped initial and final molecular states. The stationary-phase method has been used to reproduce the general features and the magnitude of the cross-section structure.

INTRODUCTION

Satellite spectra of metal atoms perturbed by foreign gases at thermal energies have been under continuous study, both experimentally[1–3] and theoretically.[4–6] In fact the theoretical understanding of the phenomenon has made possible the deduction of various interatomic potentials and transition moments from experimental photon-emission spectra.[1–3] In this article we have investigated the satellite structure produced by laser-assisted charge-transfer collisions at an energy high above thermal energies but still sufficiently low so that semiclassical approximations can be used. The two classes of studies mentioned above should complement each other in the understanding of the nature of intermolecular forces.

Our investigation indicates that various semiclassical approximations that have some success in explaining the satellite spectra at thermal energies are not adequate for moderate energy collisions. Therefore, we have derived a new formula which can explain the laser-assisted charge-transfer satellite spectra. Most significantly, the spectra on either side of the satellite frequency can be treated uniformly within the stationary-phase approximation. No *ad hoc* assumption about extending the spectra formula from the bright side (the classically accessible region) to the dark side (the classically forbidden region) has to be made.

The system which we focus on is the cross-beam charge-transfer reaction:

$$H^+ + Na(3s) + \hbar\omega \rightarrow H(n=2) + Na^+ . \quad (1)$$

The incident relative nuclear velocities are set at $v = 0.005$ and 0.01 a.u., respectively. The laser employed has a power density of 1 GW/cm^2 and a polarization vector $\mathscr{E}$ parallel to the collision velocity $\mathbf{v}$. At these velocities it is valid to use the molecular-state expansion method within the impact-parameter formalism to describe the scattering process. The calculation method used has been described in detail in a previous paper,[7] and will not be repeated here.

THEORETICAL METHOD AND RESULTS

In summary, we have solved the following coupled equations:

$$i\hbar\dot{a}_i = \epsilon_i a_i + \mathbf{v}\cdot\langle\phi_i|(\mathbf{p}+\mathbf{A})|\phi_j\rangle a_j + \sum_j \langle\phi_i|H'|\phi_j\rangle a_j + O(\mathbf{v}^2, \mathbf{v}\cdot\mathbf{A}\gamma, \mathbf{A}\gamma^2) , \quad (2)$$

where a_i is the transition amplitude to the ith Born-Oppenheimer (BO) molecular state, ϵ_i is the ith state eigenenergy, and $\langle\phi_i|(\mathbf{P}+\mathbf{A})|\phi_j\rangle$ and $\langle\phi_i|H'|\phi_j\rangle$ are the laser-induced coupling and collision-induced matrix elements, respectively. The nuclear trajectory, which is assumed to be linear, is described by

$$\mathbf{R}(t) = \mathbf{b} + \mathbf{v}t . \quad (3)$$

Finally the cross section to the ith state can be obtained through

$$\sigma_i = \int_0^\infty 2\pi b db \, |a_i|^2 . \quad (4)$$

Shown in Fig. 1 is the energy diagram of the relevant NaH^+ molecular levels. The molecular-state calculations employed the pseudopotential method and are identical to those described in Ref. 8. Note that because of the degeneracy of $H(n=2)$ states and various level crossings we have determined it is necessary to do a six-state coupled-channel calculation. In the laser-frequency range which

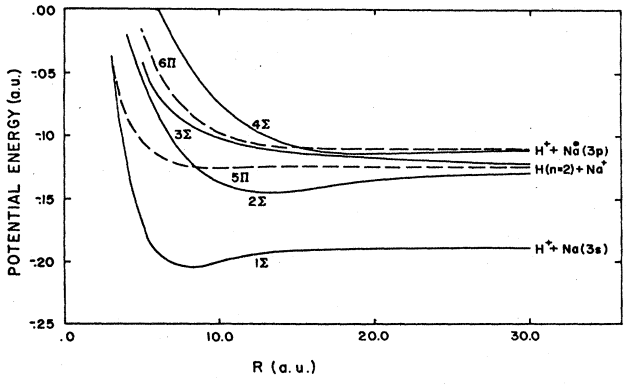

FIG. 1. Calculated potential energies for the 1Σ, 2Σ, 3Σ, 4Σ, 5Π, and 6Π BO molecular states of $(NaH)^+$.

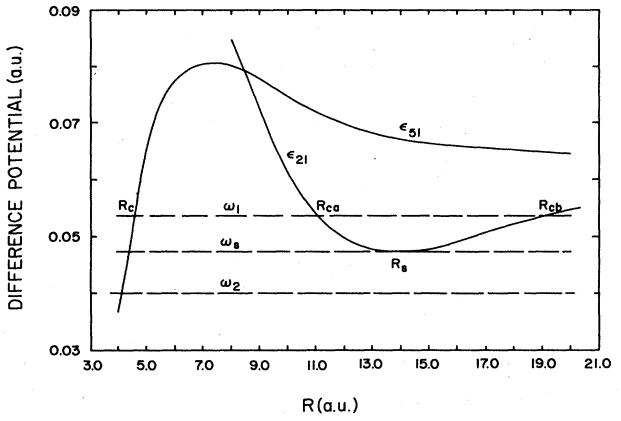

FIG. 2. Energy difference between 1Σ and 2Σ and between 1Σ and 5Π states are plotted here.

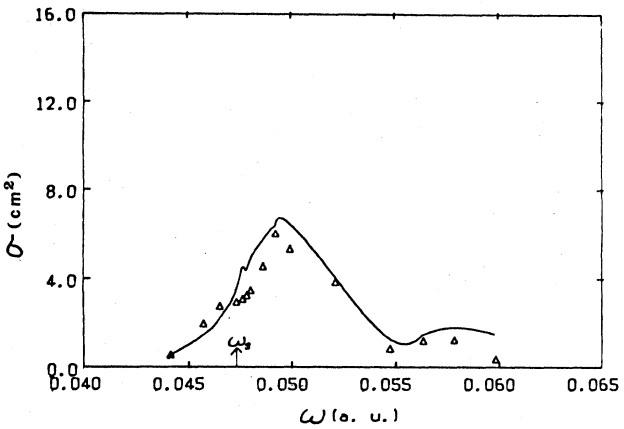

FIG. 3. Total charge-transfer cross sections for an incident nuclear velocity of 0.01 a.u. are plotted against applied laser frequencies. The triangles are the data computed through solving Eq. (2). The solid curve is due to a semiclassical approximation explained in the text.

we use, electron capture to the 2Σ and 5π states dominates the collision process. The difference potentials between the 1Σ and 2Σ states, ϵ_{21}, and between the 1Σ and 5π states, ϵ_{51}, are shown in Fig. 2. There is an extremum in ϵ_{21} located at $R_s = 13.81$ a.u., the satellite point. The magnitude of ϵ_{21} at that point is about 0.0473 a.u. For a laser frequency of $\omega_1 > \omega_s$, Fig. 2 shows that there are two resonance points, R_{ca} and R_{cb}, via which transitions to the 2Σ state are possible. At the frequency ω_s, there is only one resonance point R_s, the satellite point. For $\omega_2 < \omega_s$, there exists no resonance, and is termed the classically forbidden region. The case for transition to the 5π state is much simpler; for $\omega < 0.06$ a.u. there is only one resonance point such as R_c shown in Fig. 2.

Let us discuss the case with an incident velocity of 0.01 a.u. first. The total charge-transfer cross section to the $H(n=2)$ levels, the 2Σ, 3Σ, and 5π molecular states, was obtained by solving the coupled equations given by Eq. (2). The results are presented in Fig. 3, where the cross section is plotted against the applied laser frequency. A prominent peak located on the bright side of the satellite frequency ω_s is observed, followed by a quantum undulation. The satellite peak can be attributed to the coherence effect of two closed-by resonance points in the 1Σ to 2Σ transition. On the dark side where $\omega < \omega_s$, the cross section decays as expected exponentially. Since the computer calculation is quite time consuming, it is advantageous to derive a simple semiclassical formula that can qualitatively explain the satellite spectra.

Applying first-order perturbation theory[9] and keeping only the laser-induced terms which are dominant at low collision velocities, we can integrate Eq. (2) to obtain[10]

$$|a_i|^2 = \frac{4e^2}{\hbar^2 v^2}\left[\frac{|A_0|\omega}{c}\right]^2 \times \left|\int_b^\infty L_i(R')\cos\left[\frac{\alpha_i(R';\omega)}{\hbar v}\right]dR'\right|^2, \tag{5}$$

where

$$\alpha_i(R;\omega) = \int_b^R (\epsilon_{i1} - \hbar\omega)\frac{R'dR'}{(R'^2 - b^2)^{1/2}} \tag{6}$$

and

$$L_i(R) = \frac{\epsilon_{i1}(R)}{\hbar\omega} \times \left\{\begin{array}{c} \langle i\Sigma|z|1\Sigma\rangle \\ \text{or} \\ -\langle i\Pi|x|1\Sigma\rangle \end{array}\right\} \times \frac{b}{(R^2 - b^2)^{1/2}}. \tag{7}$$

In Eq. (7), either the transition-matrix element along the molecular axis or perpendicular to the molecular axis should be used according to whether the ith state is a Σ state or a Π state.

Since the collision velocity is low, the contribution to the phase integral in (5) comes mainly from the stationary points. Let us consider transitions to the 2Σ state first. As discussed earlier, for the transition to the 2Σ state we have two stationary points, R_{ca} and R_{cb}, if $\omega > \omega_s$. A quadratic expansion about each stationary point for the phase function α_2 leads us directly to[7]

$$|a_2|^2 \simeq \sum_{i=a,b} \frac{4\pi e^2}{\hbar v}\frac{|A_0|^2\omega^2}{c^2}|\langle 2\Sigma|z|1\Sigma\rangle|^2_{R_{ci}}\left\{\left[1 - \left[\frac{b}{R_{ci}}\right]^2\right]^{1/2} \Big/ \left|\frac{d}{dR}\epsilon_{21}\right|_{R_{ci}}\right\}, \tag{8}$$

and

$$\sigma_2 \simeq \sum_{i=a,b} \frac{8\pi^2 e^2 R_{ci}^2}{3\hbar v} \frac{|A_0|^2\omega^2}{c^2} |\langle 2\Sigma|z|1\Sigma\rangle|^2_{R_{ci}} \Big/ \left|\frac{d}{dR}\epsilon_{21}\right|_{R_{ci}} . \quad (9)$$

Note that in Eqs. (8) and (9) we have added the contribution from each stationary point incoherently. For $\omega \gg \omega_s$, Eq. (9) is adequate, but for ω close to ω_s, it begins to break down. In fact the formula fails at ω_s, where in the denominator the first derivative of ϵ_{21} is zero. Furthermore, when the two stationary points are close to each other, the coherence effect can no longer be neglected. Thus, higher-order corrections are needed.

A cubic expansion about the stationary points has been developed by Sando and Womhoudt.[4] In fact they have argued that a cubic expansion about the outer stationary point R_{cb} was sufficient because the cubic-degree expansion polynomial automatically produced a second mirror stationary point, which for ω close to ω_s should simulate the inner stationary point R_{ca}. Based on this approximation we can obtain from Eq. (5)

$$|a_2|^2 \simeq \frac{2^{11/3}\pi^2 e^2}{(\hbar v)^{4/3}} \left[\frac{|A_0|\omega}{c}\right]^2 \times |\langle 2\Sigma|z|1\Sigma\rangle|^2_{R_{cb}} \frac{A_i^2(-z)}{|\alpha^{(3)}|^{2/3}} , \quad (10)$$

where

$$\alpha^{(3)} \simeq \frac{d^2\epsilon_{21}}{dR^2}\bigg|_{R_s} \frac{R_s}{(R_s^2-b^2)^{1/2}} - \frac{d\epsilon_{21}}{dR}\bigg|_{\omega} \frac{2b^2}{(R_s^2-b^2)^{3/2}} , \quad (11)$$

$$\alpha^{(2)} \simeq \frac{d\epsilon_{21}}{dR}\bigg|_{\omega} \frac{R_s}{(R_s^2-b^2)^{1/2}} , \quad (12)$$

and

$$z \simeq \alpha^{(2)2}/[|\alpha^{(3)}|^{4/3}/(2\hbar v)^{2/3}] . \quad (13)$$

A_i is the Airy function of the first kind.[11] Note that in Eqs. (11) and (12), the trajectory factors and $d^2\epsilon_{21}/dR$ are set at R_s, the approximate midpoint between the two stationary points. This kind of averaging procedure is valid for an ω close to ω_s. If ω is very close to ω_s such that ϵ_{21} is harmonic around R_s, then

$$\frac{d\epsilon_{21}}{dR}\bigg|_{\omega} \simeq \frac{d^2\epsilon_{21}}{dR^2}\bigg|_{R_s}(R-R_s) \simeq \left[2\frac{d^2\epsilon_{21}}{dR^2}\bigg|_{R_s}\hbar(\omega-\omega_s)\right]^{1/2} . \quad (14)$$

Equation (10) was developed for $\omega \gtrsim \omega_s$. For $\omega < \omega_s$, there is no stationary point on the ϵ_{21} curve. Sando and Womhoudt then assumed Eq. (14) could be analytically continued into this region such that $(d\epsilon_{21}/dR|_{\omega})^2$ becomes negative. The Airy function then behaved like an exponentially decaying function. This assumption, which enjoys moderate success in explaining the thermal-energy spectral data, is intuitively appealing but not quite convincing. A plot of the transition cross section σ_2, obtained through Eq. (10), against the full computer result is shown in Fig. 4. As can be seen from the graph, the Sando-Womhoudt approximation is adequate only for $\omega < 0.0492$ a.u., the immediate region around ω_s. It fails to reproduce either the satellite peak or the shoulder around $\omega = 0.055$ a.u.

A second approach in using the cubic expansion method which suppresses the unwanted mirror stationary points is the uniform stationary-phase approximation (USPA) developed by Carrier.[12] The idea is to replace the Airy function $A_i(-z)$ by

$$A_i(-z) \rightarrow \tfrac{1}{2}[A_i(-z) + iB_i(-z)\mathrm{sgn}(\alpha^{(2)})] , \quad (15)$$

where B_i is the Airy function of the second kind,[11] and then sum up the contribution from each trajectory-available stationary point. Eq. (5) now becomes

$$|a_2|^2 \simeq \frac{2^{8/3}\pi^2 e^2}{(\hbar v)^{4/3}} \left[\frac{|A_0|\omega}{c}\right]^2 \left|\sum_{i=a,b} I_i\right|^2 , \quad (16)$$

where

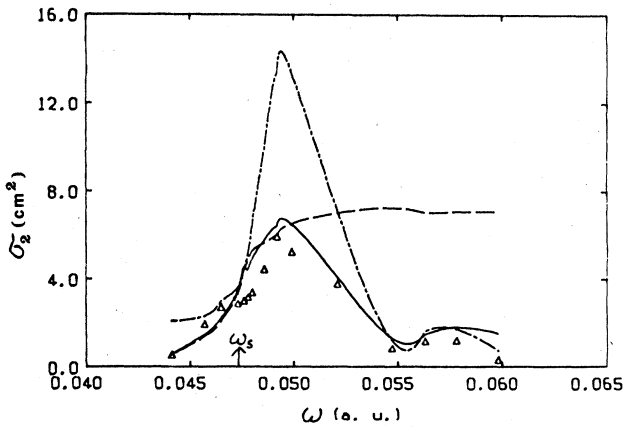

FIG. 4. Charge-transfer cross sections to the 2Σ state for an incident nuclear velocity of 0.01 a.u. are plotted against applied laser frequencies. The triangles are the computed data through solving Eq. (2). The dashed line is due to Sando-Womhoudt—type approximation using Eq. (10), the dashed-dotted line is due to USPA-type approximation using Eq. (16), and the solid line is due to a new approximation using Eq. (18).

$$I_i=\begin{cases}\dfrac{\langle 2\Sigma\,|\,z\,|\,1\Sigma\rangle}{|\,\alpha^{(3)}\,|^{1/3}}\left[\cos\left[\dfrac{\alpha}{\hbar v}\pm\zeta\right]A_i(-z)\mp\sin\left[\dfrac{\alpha}{\hbar v}-\zeta\right]B_i(-z)\right] & \text{if } b<R_{ci}\\ 0 \text{ if } b\geq R_{ci}\ . & \end{cases} \tag{17}$$

Note that the upper set of signs should be applied at R_{cb} where $d\epsilon_{21}/dR>0$, while the lower set of signs should be applied at R_{ca} where $d\epsilon_{21}/dR<0$. The parameters $\alpha^{(2)}$, $\alpha^{(3)}$, and z are similar to those in the Sando-Womhoudt case except that they are to be evaluated at each relevant stationary point R_{ci} instead of at R_s. The new parameter ζ, also to be evaluated at each R_{ci}, is defined as $\zeta=\frac{2}{3}(z)^{3/2}$.

For $\omega\gg\omega_s$, Eq. (16) will reduce to Eq. (8), a Landau-Zerner—type formula, while at $\omega=\omega_s$ it agrees with Eq. (10), the Sando-Womhoudt—type formula. For $\omega<\omega_s$, the extension of Eq. (16) using the Sando-Womhoudt analytic continuation does not produce favorable results as can be seen from Fig. 4. For $\omega>\omega_s$ the USPA method does produce qualitatively the right behavior of the cross section versus ω, although not quantitatively. It is customary to employ the Sando-Womhoudt—type formula[6] for $\omega<\omega_s$, and the USPA formula for $\omega>\omega_s$ for thermal-energy satellite spectra.

The failure of the Sando-Womhoudt—type approach hints on a new method which has been overlooked in the literature. The method is to expand the phase function α in Eq. (5), not around any stationary point but around the satellite point R_s, which sits midway between the two stationary points. Although R_s is *not* a stationary point for $\omega>\omega_s$, the cubic-degree polynomial centered at R_s does have the capacity to produce two stationary points valid for ω close to ω_s. More significantly this new type of phase-function expansion can also be applied to the case where $\omega<\omega_s$. Since this time we do not expand α_2 around any stationary point, the fact that for $\omega<\omega_s$ no stationary point exists in α_2 does not cause any conceptual problem. An expansion around R_s will therefore treat the spectra on either side of satellite frequency ω_s *on the same footing* and no assumption that analytic extension has to be made. If a cubic expansion is made about R_s, the transition probability becomes

$$|\,a_2\,|^2\simeq\frac{2^{11/3}\pi^2e^2}{(\hbar v)^{4/3}}\left[\frac{\omega_s}{\omega}\right]^2\left[\frac{|\,A_0\,|\,\omega}{c}\right]^2|\,\langle 2\Sigma\,|\,z\,|\,1\Sigma\rangle\,|^2_{R_s}\frac{1}{|\,\alpha^{(3)}\,|^{2/3}}A_i^2\left[\frac{(2\alpha^{(1)}-\alpha^{(2)2}/\alpha^{(3)})\mathrm{sgn}(\alpha^{(3)})}{(2\hbar v)^{2/3}\,|\,\alpha^{(3)}\,|^{1/3}}\right], \tag{18}$$

where $\alpha^{(1)}$, $\alpha^{(2)}$, and $\alpha^{(3)}$ are the first three derivatives of the phase function α evaluated at R_s. Note that we need the first derivative, $\alpha^{(1)}$, because R_s is not a stationary point except for $\omega=\omega_s$ at which $\alpha^{(1)}$ is zero. A plot of σ_2 using Eq. (18) for transition probability is shown in Fig. 4. The new approximation predicts well the position and the height of the satellite peak at $\omega\simeq0.0492$ a.u. and the position and the height of the shoulder at $\omega\simeq0.055$ a.u. On the dark side where $\omega<\omega_s$, the formula still agrees with the full scale numerical calculation. Beyond the first shoulder on the bright side the new formula does not agree that well with the computed data. This only reflects the fact that our formula is an expansion around $R_s(\omega_s)$, therefore we cannot expect it to perform well for $\omega\gg\omega_s$.

The case for transitions to the 5Π state is much simpler. In the frequency range that we are interested in, there is only one single resonance point which is away from its own satellite point, see Fig. 2. The USPA-type formula which is able to handle the single resonance point case should be used here. The transition cross section σ_5 is important, relative to σ_2, for $\omega<\omega_s$, because the classically forbidden region of 2Σ transition is still a classically allowed region for the 5Π transition. The total charge-transfer cross section for charge transfer to all H($n=2$) states is therefore approximately given by

$$\sigma=\sigma_2+\sigma_3+\sigma_5\approx\sigma_2[\text{based on Eq. (18)}]+\sigma_5[\text{based on Eq. (16)}]\ . \tag{19}$$

The results of using Eq. (19) are plotted in Fig. 3 where they are compared with the computed total charge-transfer cross section to the H($n=2$) states. The agreement is good up to the first shoulder point where

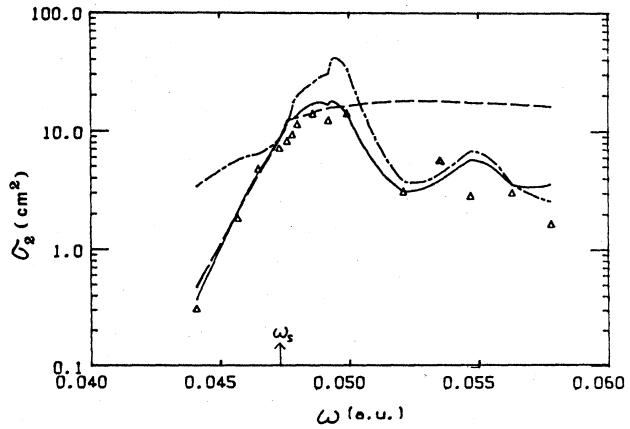

FIG. 5. Charge-transfer cross sections to the 2Σ state for an incident nuclear velocity of 0.005 a.u. are plotted against applied laser frequencies. The triangles are the computed data obtained by solving Eq. (2). The dashed line is due to Sando-Womhoudt—type approximation using Eq. (10), the dashed-dotted line is due to USPA-type approximation using Eq. (16), and the solid line is due to a new approximation using Eq. (18).

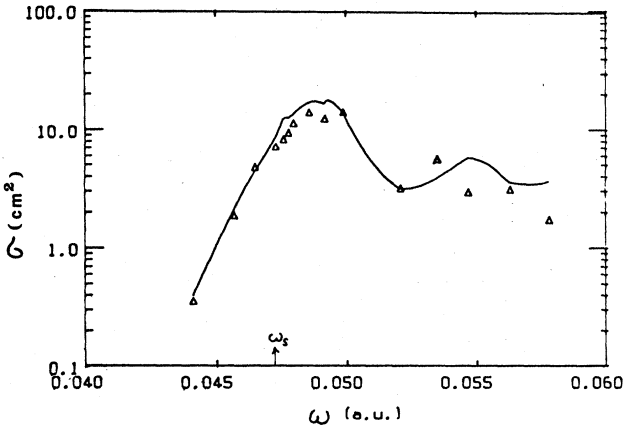

FIG. 6. Total charge-transfer cross sections for an incident nuclear velocity of 0.005 a.u. are plotted against applied laser frequencies. The triangles are the data computed through solving Eq. (2). The solid curve is due to a semiclassical approximation explained in the text.

$\omega \simeq 0.055$ a.u. Note that the magnitude of σ_5 is only $\sim 10\%$ that of σ_2 at $\omega = 0.441$ a.u., the first data point shown.

Lowering the incident nuclear velocity will have two effects on the satellite spectra. First of all, a lower nuclear velocity means that it takes longer for the colliding system to travel through the resonance regions, and therefore a larger charge-transfer cross section for $\omega > \omega_s$ can be realized. On the other hand, the more stringent requirement of observing the "resonance condition" will further suppress the cross section for $\omega < \omega_s$. Thus, we expect a faster drop of the cross section from the satellite peak to the first shoulder on the spectroscopic bright side. We shall also see a closer shoulder to the satellite point ω_s. All these predictions are born out by the calculational results given in Figs. 5 and 6, where the charge-transfer cross section for the incident velocity of 0.005 a.u. is displayed.

Figure 5 shows that the analytical formula we derived, Eq. (18), predicts the height and the position of the satellite peak quite well; the charge-transfer cross section to the 2Σ state has a peak of 14×10^{-16} cm^2, occurring around $\omega = 0.092$ a.u. Equation (18) also describes well the magnitude and the position (around $\omega = 0.0521$ a.u.) of the first shoulder. However, the Sando-Womhoudt—type approximation, Eq. (10), agrees with the computed data only in the vicinity of the satellite points ω_s. It fails either to predict the existence of a shoulder in the spectra or to describe the computed data for the region where $\omega < 0.0457$ a.u., the deep classically forbidden region. The USPA-type approximation, Eq. (16), again only qualitatively explains the bright-side data and fails completely in explaining the dark-side spectra.

As for the total charge-transfer cross section shown in Fig. 6, Eq. (19) which we derived earlier, describes the spectra reasonably well. Note that at $\omega = 0.0441$ a.u., the first data point shown, the contribution from the 5Π transition makes up a larger percentage (about 15%) of the total charge-transfer cross section than before. This is due to the fact that a lower incident velocity suppresses more the classically forbidden 2Σ transition.

In conclusion, we believe that we have derived a new formula which is able to treat the spectra on either side of the satellite frequency uniformly. It is capable of describing the spectra near the satellite frequency while other type approximations fail to do so, at least at the collision energies we have studied. This comparison indicates that the new method may be a better tool for the experimental deduction of important intermolecular data.

ACKNOWLEDGMENTS

The authors want to thank Dr. R. J. Bieniek for an introduction to molecular satellite spectra. This work was supported by the Office of Fusion Energy of the Department of Energy.

[1]C. G. Carrington and A. Gallagher, Phys. Rev. A **10**, 1464 (1974).

[2]B. Sayer, M. Ferray, J. P. Visticot, and J. Lozingto, J. Phys. B **13**, 177 (1980).

[3]C. Bousquet, N. Bras, and Y. Majdi, J. Phys. B **17**, 1931 (1984).

[4]K. M. Sando and J. C. Womhoudt, Phys. Rev. A **7**, 1889 (1973).

[5]J. Szudy and W. E. Baylis, J. Quant. Spectrosc. Radiat. Transfer **15**, 641 (1975).

[6]R. J. Bieniek and T. J. Streeter, Phys. Rev. A **28**, 3328 (1983).

[7]Y. P. Hsu, M. Kimura, and R. E. Olson, Phys. Rev. A **31**, 576 (1985).

[8]M. Kimura, R. E. Olson, and J. Pascale, Phys. Rev. A **26**, 3113 (1982).

[9]The applicability of the first-order approximation can be checked by asking whether the cross section computed varies linearly with the laser-power density.

[10]We define the vector potential **A** for the laser field as $\mathbf{A}\gamma = 2 \mid A_0 \mid \cos(\omega t)$.

[11]*Handbook of Mathematical Functions,* Natl. Bur. Stand. (U.S.) Appl. Math. Ser. No. 55, edited by M. Abramowitz and I. A. Stegun (Dover, New York, 1965).

[12]G. F. Carrier, J. Fluid Mech. **24**, 641 (1966); also see the appendix of W. H. Miller, J. Chem. Phys. **53**, 3478 (1970).